



Quantifying the Impact of Site and Path Effects on the Rapid Estimation of Source Parameters

Quan Dong*

Key Laboratory of Earthquake Engineering and Engineering Vibration, Institute of Engineering Mechanics, China Earthquake Administration; Key Laboratory of Earthquake Disaster Mitigation, Ministry of Emergency Management, Harbin, 150080

dongquan233233@163.com

Abstract. Local site conditions significantly influence ground motion and are critical for earthquake engineering and geotechnical earthquake engineering. Earthquake early warning systems (EEWs) typically rely on early ground acceleration records to estimate magnitude, which are inevitably affected by site effects. Recently, a method for measuring source parameters in the time domain has been proposed, showing potential for application in earthquake early warning. This study investigates the influence of local site conditions and propagation paths on this new method in EEWs, utilizing a dataset from 96 earthquakes with $MW \geq 5.5$ recorded by KiK-net in Japan. The results indicate that the effects of site response on moment magnitude, corner frequency, and stress drop are noticeably weakened. Particularly, as earthquake magnitude increases, the influence of site effects on the measured source parameters gradually diminishes. Additionally, path effects generally have a limited impact on the estimation of source parameters from the new method. This research provides a quantitative evaluation method for determining source parameters in earthquake early warning systems and offers significant insights into enhancing parameter estimation accuracy in practical applications.

Keywords: source parameters; site effect; path effect; site classification; time-domain method

1 Introduction

Site effects refer to the amplification or attenuation of seismic wave amplitudes caused by variations in site-specific soil characteristics during seismic wave propagation, directly influencing ground motion characteristics and the severity of earthquake damage^[1]. Accurately quantifying site effects is essential not only for estimating source parameters but also for ensuring the reliability of ground motion prediction models and enhancing seismic hazard mitigation decisions^[2]. In recent years, advancements in seismic observation technology, particularly the establishment of extensive strong-motion observation networks such as Japan's KiK-net, have provided abundant data resources for in-depth studies of site effects. Rapid and accurate estimation of source parameters

is crucial in earthquake engineering and disaster assessment, and site effects can significantly impact these parameters. Therefore, quickly estimating the influence of site effects on source parameters plays a crucial role in improving the response efficiency of earthquake monitoring and post-disaster assessments^[3].

However, current research on the effects of site and path conditions on source parameters is largely confined to single events or simplified models and has not comprehensively quantified the specific influences of various magnitudes and site types^{[4][5]}. Several key issues remain unresolved in current studies: firstly, many studies do not adequately account for the influence of different site types on source parameter estimation; secondly, existing studies, whether employing parametric or non-parametric methods for estimating source parameters, generally rely on post-event collected records that require converting time-domain signals to frequency-domain analysis, making rapid estimation of site and path effects challenging. Finally, existing studies often rely on simplified single-source models and lack comprehensive analyses of complex propagation paths and site effects during actual seismic events. Kaneko and Shearer highlighted that the geometry of the seismic source significantly impacts the uncertainty of estimating parameters such as stress drop and corner frequency^[6]. Current research predominantly focuses on small to moderate seismic events, utilizing a "circular fault" source model, which is unsuitable for moderate to large earthquakes, where fault rupture propagation distances exceed fault width.

Path effects refer to seismic wave attenuation and spectral changes along propagation paths, potentially causing biases in source parameter estimation. Currently, research on path effects is relatively limited, and there remains debate over whether path effects need explicit consideration in rapid estimation methods.

Given these issues, this study utilizes strong-motion seismic data ($M_w \geq 5.5$) from Japan's KiK-net network, employing a rapid source parameter estimation method based on the time-domain root mean square (RMS) of ground motion, which is suitable for real-time earthquake early warning systems. This research systematically quantifies the influences of site and path effects. The objectives are to: (1) clarify how site effects specifically influence source parameters across different magnitude ranges; (2) analyze how various site types affect source parameter estimation results; (3) investigate the contributions of path effects in source parameter estimation.

This study innovates methodologically and analytically by: first, systematically quantifying site effects on source parameters across different magnitude ranges; second, explicitly defining the role and limitations of path effects in rapid source parameter estimation. These contributions not only enhance the theoretical framework for rapid source parameter estimation but also provide reliable data support and scientific evidence for the development and practical implementation of earthquake early warning systems.

2 Data

2.1 Data Source

Historical earthquake damage surveys have shown that local site conditions significantly affect seismic ground motion characteristics and the severity of earthquake-induced damage. Regional site effect studies for quantitative evaluations of site-specific conditions rely heavily on detailed borehole profiles or strong-motion records[7]. Japan's National Research Institute for Earth Science and Disaster Resilience (NIED) established the KiK-net strong-motion observation network, with each station equipped with high-sensitivity, three-component accelerometers installed at both the surface and in boreholes. Additionally, KiK-net provides detailed borehole information, including soil layer structures and shear-wave velocity profiles. Given these advantages and the objectives of this study, the dataset utilized in this research was sourced from Japan's KiK-net strong-motion observation network.

To ensure data representativeness and mitigate temporal clustering, earthquake records spanning from 2000 to 2024 with moment magnitudes $M_w \geq 5.5$ and focal depths less than 60 km were selected, totaling 96 seismic events. Earthquakes with magnitudes ranging from 5.5 to 6.5 included records within 100 km epicentral distances; for magnitudes between 6.6 and 6.9, records within 150 km were selected; for events with magnitudes equal to or greater than 7.0, records within 200 km were included. After visually inspecting and removing abnormal records triggered after the P-wave arrival, records with indistinguishable P-wave arrivals due to noise, and incomplete station information, a final dataset of 2000 valid strong-motion records was obtained. Each record set comprises two horizontal and one vertical component from both surface and borehole sensors. Catalog moment magnitudes ($M_{w_{cata}}$) of seismic events were obtained from the Global Centroid Moment Tensor Project (www.globalcmt.org). The spatial distributions of earthquake epicenters (circles) and recording stations (triangles) are shown in Figure 1. Distributions of epicentral distance and moment magnitude for each strong-motion record are illustrated in Figure 2.

2.2 Data Processing

Data processing began with baseline correction by subtracting the mean value of the initial 5 seconds from raw acceleration records. Subsequently, the P-wave arrivals were automatically identified using a combination of the Short-Term Average to Long-Term Average (STA/LTA) method and the Akaike Information Criterion (AIC) method^[8], followed by manual inspection and adjustments. The theoretical difference between P- and S-wave arrival times was utilized to estimate S-wave arrivals, with 90% of the theoretical difference adopted as the actual arrival time difference, using wave velocities of $C_p = 5333$ m/s for P-waves and $C_s = 3200$ m/s for S-waves. After baseline correction, the acceleration records were integrated once and twice to obtain velocity and displacement time histories, respectively. A bidirectional Butterworth high-pass filter (with a low-frequency cutoff 0.02 Hz) was then applied to filter the velocity and displacement time histories. Finally, the three components of acceleration, velocity, and

displacement time histories were separately substituted into Equation to calculate the root mean square (RMS) of ground motion.

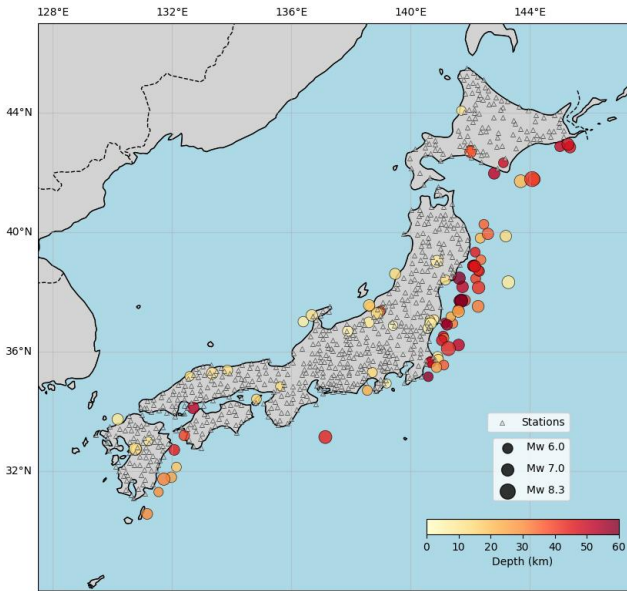


Fig. 1. Distribution Map of the Earthquake Epicenter and Stations.

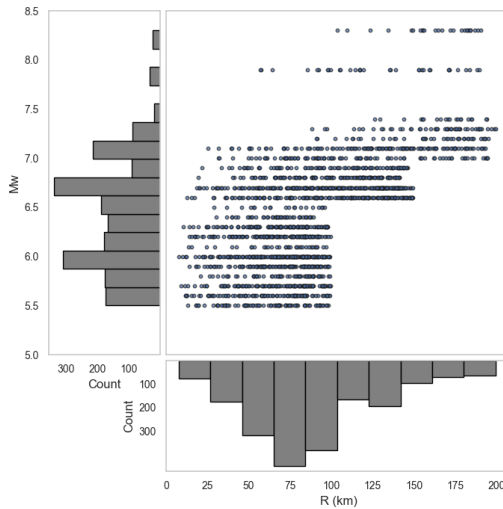


Fig. 2. Distribution Map of Recorded Magnitudes and Epicentral Distances.

$$P_{rms} = \sqrt{\sum_{i=1}^n (UD_i^2 + NS_i^2 + EW_i^2)/n} \quad (1)$$

In Equation (1), parameter P_{rms} represents the acceleration root mean square A_{rms} , velocity root mean square V_{rms} , and displacement root mean square D_{rms} . UD , NS , and EW indicate vertical, north-south, and east-west ground motions, respectively. The parameter n represents the number of sampling points in the input records. Compared to acceleration and velocity, displacement time histories are more sensitive to low-frequency components, requiring a correction for low-frequency components in displacement RMS parameters. Therefore, the correction method proposed by Lior and Ziv^[9] was applied, yielding the corrected displacement RMS \hat{D}_{rms} as given by Equation (2).

$$\hat{D}_{rms} = \sqrt{(D_{rms})^2 + (D_{rms}^{corr})^2} \quad (2)$$

Where D_{rms} is the previously obtained displacement RMS, and D_{rms}^{corr} is the low-frequency correction term, calculated as shown in Equation (3).

$$D_{rms}^{corr} = \sqrt{\frac{2}{\pi}} D_{rms} \sqrt{\left[\frac{f_0 f_c}{f_0^2 + f_c^2} + \tan^{-1} \left(\frac{f_c}{f_0} \right) \right]} \quad (3)$$

Where, $f_c = \max(1/T, f_1)$ is the cutoff frequency of the missing signal, T is the duration of the record.

3 Method for Calculating Source Parameters

Considering that this study focuses on moderate to large earthquakes ($M_W \geq 5.5$), the rupture process is constrained by crustal thickness, resulting in rupture lengths along the fault strike generally exceeding fault widths. The conventional circular source model does not accurately characterize the rupture surface of moderate to large earthquakes. Therefore, this study adopts a time-domain RMS seismic motion method for source parameter estimation based on an elliptical source model suitable for moderate to large earthquakes. Compared to traditional frequency-domain methods such as spectrum inversion, which require converting time-domain signals into frequency-domain representations before estimating source parameters, the time-domain method has distinct advantages. One of the major benefits of the time-domain method is its real-time processing capability. Unlike frequency-domain methods, which involve time-consuming transformations from time to frequency space, the time-domain RMS method can directly calculate source parameters from raw seismic waveforms, significantly reducing computational time and improving response speed, especially crucial in earthquake early warning systems, allowing rapid and reliable calculation of seismic moment, stress drop, and corner frequency using P-waveforms^[10]. Furthermore, the time-domain method requires fewer computational resources and avoids the complexities associated with spectral inversion, which can be sensitive to noise and other disturbances in the signal. By calculating parameters directly from time-domain records, this method demonstrates enhanced robustness in noisy or complex seismic environments, making

it more efficient and reliable in practical applications. The seismic moment M_0 , stress drop $\Delta\tau$, corner frequency f_0 , and the constant C_M in the equations are calculated as follows:

$$M_0 = C_M RT^{0.5} \frac{D^{1.5} V_{rms}^{1.5}}{V_{rms}^{0.5}} \quad (4)$$

$$\Delta\tau = \frac{1}{4\pi^{5.5}} C_M RT^{0.5} \frac{V_{rms}^{2.5}}{D^{1.5}} (kC_S)^{-3} \quad (5)$$

$$f_0 = \frac{1}{2\pi} \frac{V_{rms}}{D_{rms}} \quad (6)$$

$$C_M = \frac{8\pi\rho C^3}{U_{\phi\theta} F_S} \quad (7)$$

Parameters involved in the above equations are listed in [错误!未找到引用源。](#). By substituting the RMS ground motion parameters calculated from progressively increasing waveform windows after the P-wave arrival of each record into Equations (4–7), the variations of source parameters such as seismic moment, stress drop, and rupture area during the rupture evolution in the P-wave window are obtained. The seismic moment M_0 calculated is then converted to moment magnitude M_W using Equation (8). An example illustrating the calculation process of source parameters for each set of strong-motion records is shown in Figure 3.

$$M_W = (\log_{10}(M_0) - 9.1)/1.5 \quad (8)$$

The KiK-net borehole instruments are typically installed in bedrock conditions, meaning their records theoretically contain only source and propagation path information, and can thus be treated as unaffected by site effects. As illustrated by the calculation example for the representative station shown in Figure 3, differences exist between surface- and borehole-derived source parameters (moment magnitude, stress drop, and corner frequency). To quantify the influence of site effects on the rapid estimation of source parameters, this study first calculated the surface and borehole source parameters for each strong-motion record in the selected dataset. By analyzing the ratio of surface-to-borehole source parameters (moment magnitude, stress drop, and corner frequency) for each record, the site effects could be quantitatively assessed.

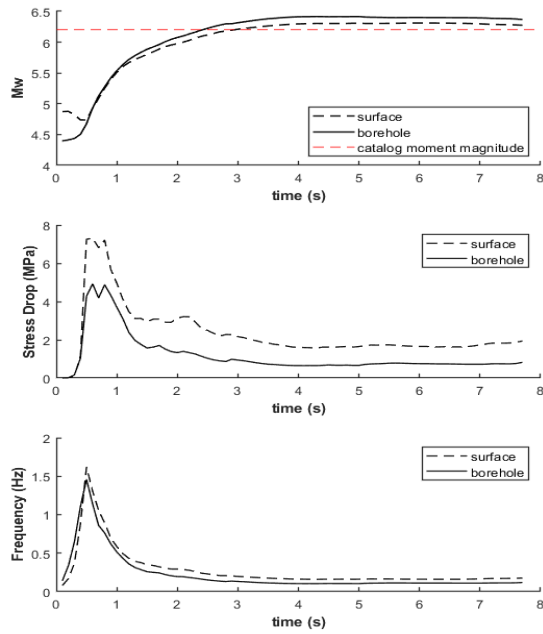


Fig. 3. Comparison of Source Parameters at the HYG15 Station for the M_w 6.2 Earthquake.

Table 1. Values Used for Calculating Source Parameters.

Parameter
$\kappa_0 = 0.025s$
$\rho = 2600kg/m^3$
$C_p = 5333m/s$
$C_s = 3200m/s$
$U_{\phi\theta}=0.52(P \text{ wave})$
$U_{\phi\theta}=0.63(S \text{ wave})$
$F_S=2$
$k = 0.34(P \text{ wave})$
$k = 0.26(S \text{ wave})$

4 Results and Discussion

The core objective of this study is to quantitatively analyze the impact of site and path effects on the rapid estimation of earthquake source parameters. Based on the methods described above, this section presents a detailed analysis from three perspectives:

magnitude groups, detailed site classifications, and path effects, to clarify the contribution of each factor to the estimation results of source parameters.

4.1 Influence of Magnitude on Source Parameters

To thoroughly investigate the effect of earthquake magnitude on site effects, seismic data were classified into three magnitude ranges: moderate earthquakes (5.5–6.5), moderately strong earthquakes (6.6–6.9), and strong earthquakes (7.0+). For each magnitude interval, the ratios of surface-to-borehole estimates of moment magnitude (M_W), corner frequency (f_0), and stress drop ($\Delta\tau$) were computed. The distribution characteristics of these ratios are illustrated using boxplots (Figure 4 and Figure 5). Each boxplot depicts the mean, median, and upper and lower quartiles for the respective magnitude groups.

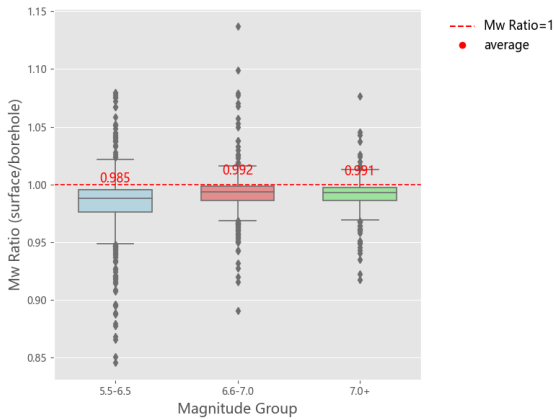


Fig. 4. Distribution of M_W Ratio Grouped by Magnitude.

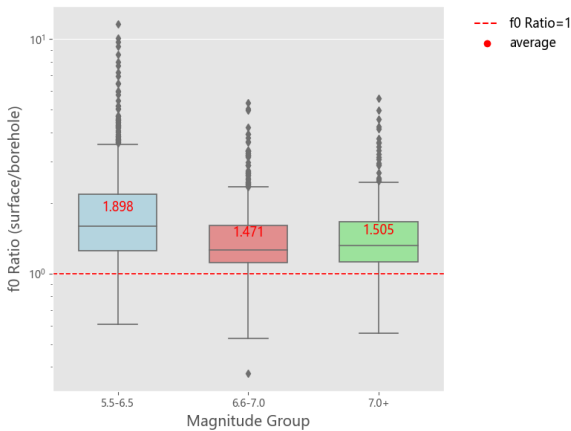


Fig. 5. Distribution of f_0 Ratio Grouped by Magnitude.

Figure 4 and Figure 5 shows that the ratios of M_W across all three magnitude groups are consistently close to 1, with median and mean values mostly ranging between 0.98 and 0.99, indicating slightly smaller moment magnitudes estimated from surface recordings compared to borehole recordings. Outliers primarily cluster narrowly below 0.95 and above 1.05, exhibiting minimal variation among different magnitude groups. These results indicate that the M_W ratios are relatively stable and unaffected significantly by site effects, suggesting the influence of site effects on M_W estimations can be considered negligible. Regarding the f_0 ratios, for the moderate magnitude group (5.5–6.5), the amplification of high-frequency components by site effects is somewhat pronounced (higher f_0 ratios). However, as the earthquake magnitude increases, the contribution of high-frequency components diminishes, causing a gradual decrease in the amplification effect. Consequently, the corner frequency ratios stabilize around approximately 1.5. This aligns well with the saturation phenomenon of nonlinear soil response typically observed at larger magnitudes.

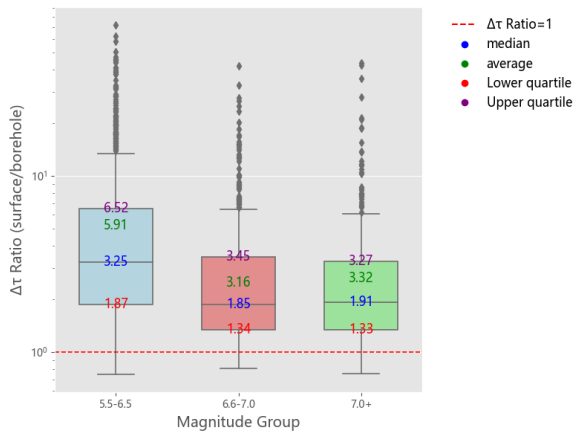


Fig. 6. Distribution of $\Delta\tau$ Ratio Grouped by Magnitude.

Figure 6 clearly reveals the impact of site effects on the stress drop ($\Delta\tau$). For moderate earthquakes (magnitude range 5.5–6.5), the ratio of surface-to-borehole stress drop is notably high (mean = 3.25, median = 5.91), with extreme individual values reaching 60–70 times. This indicates that surface-recorded stress drops are significantly higher than those recorded in boreholes, emphasizing the prominent amplification effect of local site conditions on high-frequency signals for moderate earthquakes. However, as earthquake magnitude increases, this ratio declines notably and stabilizes (mean = 3.32 and median = 1.91 for large earthquakes), reaffirming that the influence of site effects on stress-drop estimation diminishes with increasing magnitude.

This behavior likely arises because the impact of site effects (e.g., soil types and source-to-station distance) on seismic signals may be nonlinear and highly pronounced in amplifying high-frequency components for moderate events, causing stress-drop values derived from surface records to become significantly higher than those from borehole records, thus increasing the ratio. As earthquake magnitude increases, nonlinear

soil responses approach saturation, and low-frequency seismic signals dominate in large earthquake sources. Consequently, site amplification gradually weakens, reducing the difference in stress drop between surface and borehole recordings and thereby decreasing the ratio.

4.2 Influence of Site Types on Source Parameter Estimations

To further explore the influence of site types on the results discussed above, this study adopted the site classification criteria from Japanese standards based on the fundamental site period $T[11]$. The specific classification criteria, including corresponding ranges for fundamental site periods T and shear-wave velocities V_{S30} , are listed in Table 2. Site classification methods. In Table, SC I, II, III, and IV represent site categories corresponding to rock, hard soil, medium-hard soil, and soft soil, respectively. The weighted-average shear-wave velocity method used to calculate the site period is given by Equation (9):

$$T_s = \frac{4H}{V_{site}} \quad (9)$$

In Equation (9), thickness H represents the total thickness of soil layers with shear-wave velocities less than 760 m/s. The weighted-average shear-wave velocity of the site, V_{site} , is calculated using Equation (10):

$$V_{site} = \frac{H}{\sum_{i=1}^n \frac{H_i}{V_{si}}} \quad (10)$$

where H is the total thickness of the overlying soil layers (i.e., the sum of all soil layer thicknesses: $H = \sum_{i=1}^n H_i$); H_i is the thickness of the i th soil layer; V_{si} is the shear-wave velocity of the i th soil layer; and n represents the total number of soil layers.

Table 2. Site classification methods.

Site Type	Period	V_{S30} (m/s)
SC I	$T < 0.2s$	$V_{S30} > 600$
SC II	$0.2 \leq T < 0.4s$	$300 < V_{S30} \leq 600$
SC III	$0.4 \leq T < 0.6s$	$200 < V_{S30} \leq 300$
SC IV	$T \geq 0.6s$	$V_{S30} \leq 200$
SC IV1	$0.6 \leq T < 1.0s$	$120 < V_{S30} \leq 200$
SC IV2	$T \geq 1.0s$	$V_{S30} \leq 120$

Figure 7 shows the distribution of stations across different site categories, and Figure 8 illustrates the sample distributions of site types within each magnitude group. After further subdividing the site types, the ratios of surface-to-borehole moment magnitudes remain stable across different site categories (ratios consistently close to 1), indicating that site classification has minimal impact on moment magnitude estimations. The f_0 ratios also remain relatively stable across site types. Regarding the stress-drop ($\Delta\tau$)

ratios, particularly in the magnitude range 5.5–6.5, notable increases are observed in site categories SC II, SC III, and SC IV, clearly indicating that softer sites significantly amplify high-frequency components.

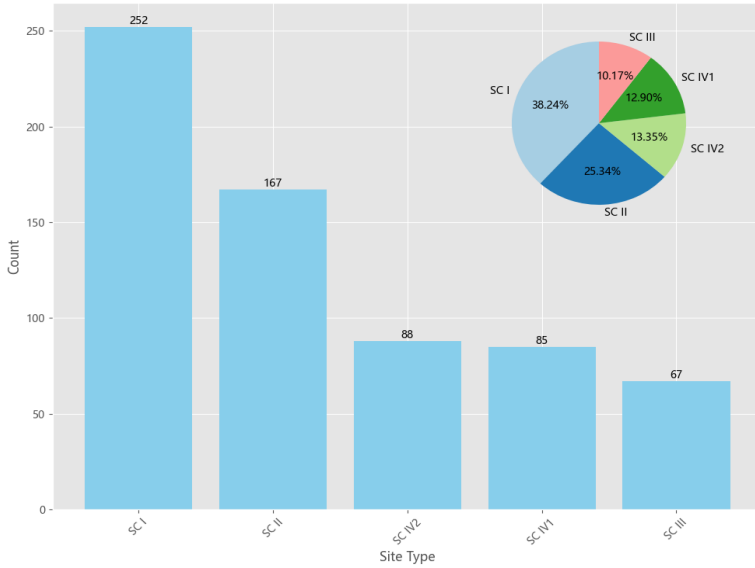


Fig. 7. Number and Proportion of Each Site Type at Stations.

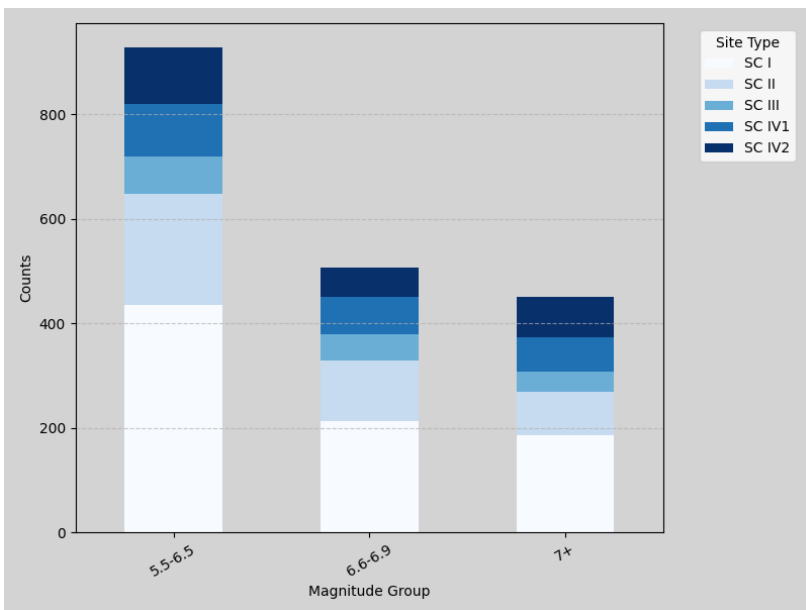


Fig. 8. Distribution of Sample Counts for Each Site Type within Each Magnitude Group.

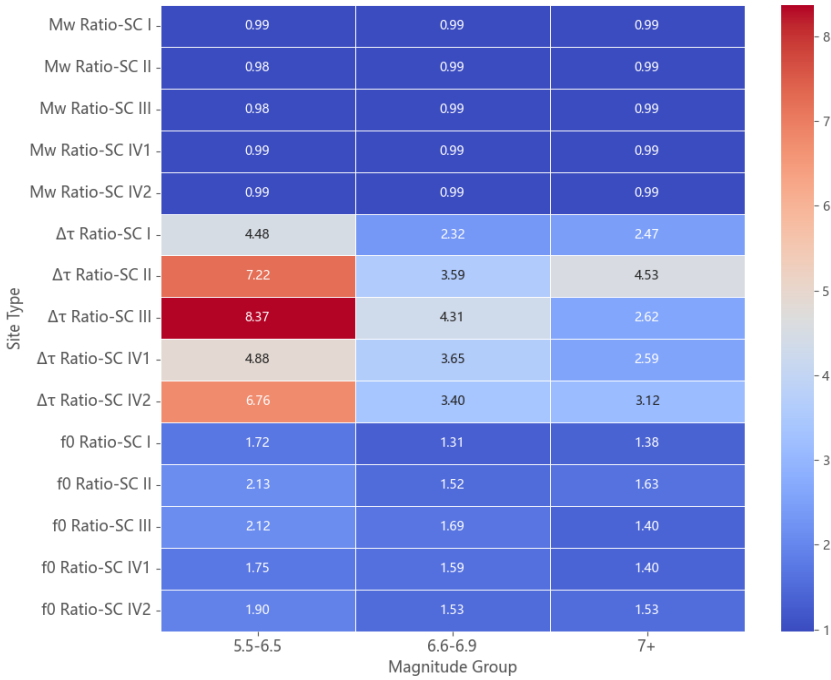


Fig. 9. Surface/Underground Source Parameter Ratios for Each Group.

Figure 9 shows the mean surface-to-borehole ratios of source parameters across each subgroup, demonstrating that the influence of site classification on the M_W ratios is negligible, while the f_0 ratios also remain relatively stable across different site types. As for the stress-drop ($\Delta\tau$) ratios, substantial amplification occurs in the magnitude range of 5.5–6.5 under SC II, SC III, and SC IV site conditions. As magnitude increases, the differences in stress-drop ratios across various site categories gradually decrease, further confirming the saturation effect of nonlinear site responses at larger magnitudes. This finding provides valuable reference for incorporating site-specific considerations into stress-drop estimations in earthquake early-warning systems. Additionally, path effects may also impact the estimation of source parameters. Due to direct proximity to the source, borehole recordings experience minimal path effects, whereas surface recordings are influenced by both propagation paths and surface heterogeneity, making path effects more pronounced in smaller earthquakes. This phenomenon amplifies differences between surface and borehole recordings. In the following section, we discuss the specific influences of path effects in detail.

4.3 Influence of Path Effects

In seismology, path effects refer to variations in seismic wave amplitudes, spectra, and ground-motion characteristics caused by differences in propagation paths during seismic wave travel^{[12][14]} Path effects impact the estimation of earthquake source

parameters in several ways, particularly through propagation distance, often causing biases in the estimated source parameters. To enhance the accuracy of source parameter estimations, it is essential to comprehensively consider path effects. In this study, the epicentral distance (distance between the earthquake epicenter and recording station) is used as a representative indicator of path effects to analyze its specific contributions to the estimation of source parameters.

Figure 10 presents the combined influence of epicentral distance and earthquake magnitude on the estimation of moment magnitude, stress drop, and corner frequency in the form of three-dimensional scatter plots. Scatter point colors indicate the magnitude of the corresponding parameters, and trend-fitting planes have been added to clarify the joint trend characteristics of path effects and earthquake magnitude.

As observed from Figure 10, estimated moment magnitudes show a strong positive correlation with catalog moment magnitudes (horizontal axis), demonstrating that the proposed estimation method is stable, accurate, and aligns closely with catalog magnitudes. Additionally, the fitted plane indicates no significant deviation in estimated moment magnitude values with increasing epicentral distance, reflecting stability and minimal influence from path effects. Thus, path-effect corrections for moment magnitude estimation are unnecessary in practical applications.

For stress drop estimates, Figure 10 indicates a clear increase with rising earthquake magnitude, emphasizing that stress drop estimation is primarily controlled by magnitude. Although the overall stress drop shows no distinct increasing or decreasing trend with increasing epicentral distance, scattered results in far-field regions suggest potential uncertainties. Thus, while path effects have limited overall influence, caution should be exercised in stress-drop estimations at greater distances.

The lower plot in Figure 10 demonstrates a clear negative correlation between corner frequency and earthquake magnitude, confirming that larger earthquakes predominantly release energy in low-frequency bands, consistent with classical earthquake source spectra theory. With increasing epicentral distance, the corner frequency exhibits a slight decreasing trend, attributed to the attenuation of high-frequency seismic waves over long propagation paths. The noticeable dispersion of corner frequency values at shorter distances suggests complexity in near-field path effects, potentially associated with local geological heterogeneities along seismic wave paths.

Overall, the results suggest that specific path-effect corrections are not necessary in the rapid estimation of earthquake source parameters, especially for large seismic events. This conclusion facilitates rapid response in practical earthquake early warning systems^[15].

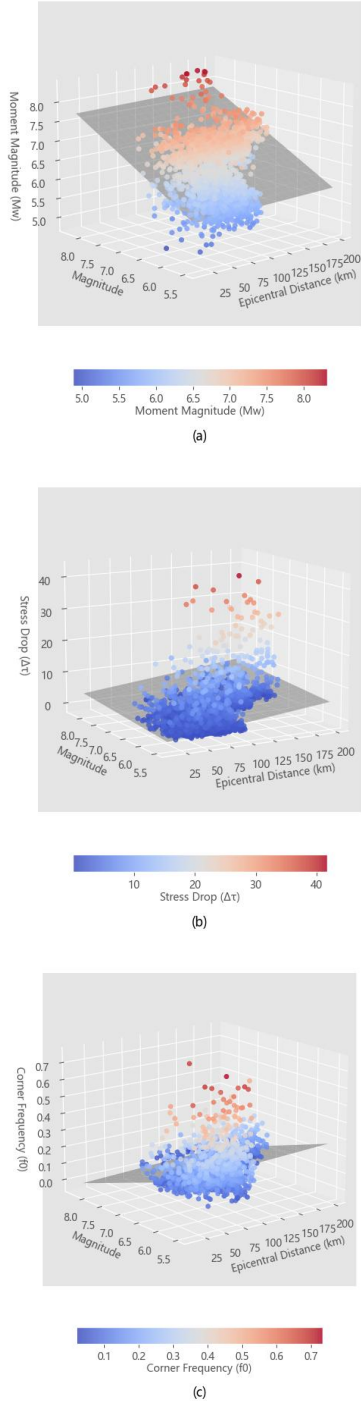


Fig. 10. (a)~(c).Statistical Relationship Between Source Dis-tance and Source Parameter

5 Conclusions and Future Prospects

Based on strong earthquake records from the KiK-net network in Japan, systematically investigates the quantitative impact of site effects and path effects on the rapid estimation of source parameters using time-domain ground motion RMS methods. The data from 96 earthquake events that occurred between 2000 and 2024 were analyzed, and the moment magnitude, stress drop, and corner frequency corresponding to surface and underground records were calculated. By comparing the surface and underground source parameters, a method for quickly quantifying site effects was proposed. In addition, the study also conducted a detailed analysis of the influence of epicentral distance to assess the contribution of path effects on source parameter estimation. The main conclusions of the study are as follows:

Moment magnitude estimation is relatively stable, with the surface and underground record ratio close to 1, indicating that site effects have limited impact on the rapid estimation of moment magnitude. The estimated moment magnitude does not show significant differences across different site types, suggesting that site type has minimal influence on moment magnitude estimation.

The influence of site effects varies significantly across different magnitude ranges. In small-magnitude events (5.5-6.5), the stress drop values derived from surface records are significantly higher than those from underground records, indicating a pronounced amplification of high-frequency ground motion by site conditions in smaller earthquakes. As the magnitude increases, particularly in large-magnitude events (greater than 6.5), the impact of site effects on stress drop diminishes, and the differences between surface and underground records significantly decrease. This suggests that source characteristics dominate the parameter estimation in large earthquakes, and the site amplification effect becomes saturated.

Path effects have a limited impact on source parameters. Analysis of the relationship between epicentral distance and source parameters revealed that path effects have a relatively limited impact on source parameters. Particularly in medium to large earthquakes, path effects do not significantly influence the estimation of moment magnitude and stress drop. This finding indicates that in practical earthquake early warning systems, the error introduced by path effects in rapid source parameter estimation is within an acceptable range, and it is not necessary to apply a separate correction for path effects.

In conclusion, the rapid quantification method for site effects proposed in this study, based on the surface/underground parameter ratio, effectively improves the efficiency and reliability of source parameter estimation. The results suggest that once preliminary estimations of moment magnitude and stress drop are obtained, they can be directly applied in ground motion prediction equations (GMPE) for the real-time estimation of peak ground acceleration (PGA) and peak ground velocity (PGV), providing a more efficient and convenient method for determining source parameters in earthquake early warning systems. Therefore, the findings of this study not only provide timely and reliable technical support for earthquake disaster assessment and emergency response but also offer important scientific references for improving parameter estimation accuracy in practical applications of earthquake early warning systems. Although the method

proposed in this study demonstrates good practicality and reliability for rapid source parameter estimation, there is still room for improvement in precision. Future research can further incorporate multi-source models to improve the source parameter estimation algorithm, especially in complex seismic source regions, to enhance estimation accuracy. This study only considers seismic source models and propagation path effects. However, real seismic environments involve additional complexities, such as non-linear seismic wave propagation effects, source heterogeneity, and deep geological structures. In the future, with the further improvement of the earthquake observation network and the continuous optimization and development of seismic source models, it is expected that the accuracy and timeliness of seismic source parameter estimation will be further enhanced, ultimately improving the rapid response capability and disaster mitigation level for earthquake disasters.

References

1. Kumar, R., Mittal, H., Sandeep, et al., "Earthquake Genesis and Earthquake Early Warning Systems: Challenges and a Way Forward," *Surveys in Geophysics*, 43(4):1143-1168, 2022, doi: 10.1007/s10712-022-09710-7.
2. Lior, I., Ziv, A., "The Relation Between Ground Motion, Earthquake Source Parameters, and Attenuation: Implications for Source Parameter Inversion and Ground Motion Prediction Equations," *Journal of Geophysical Research: Solid Earth*, 123(7):5886-5901, 2018, doi:10.1029/2018JB015504.
3. Kumari, R., Kumar, P., Kumar, N., et al., "Implications of Site Effects and Attenuation Properties for Estimation of Earthquake Source Characteristics in Kinnaur Himalaya, India," *Pure and Applied Geophysics*, 178:4345-4366, 2021, doi: 10.1007/s00024-021-02872-2.
4. Chang, H., Abercrombie, R. E., Nakata, N., et al., "Quantifying Site Effects and Their Influence on Earthquake Source Parameter Estimations Using a Dense Array in Oklahoma," *Journal of Geophysical Research: Solid Earth*, 128(9):e2023JB027144, 2023, doi:10.1029/2023JB027144.
5. Wang, J., Ma, Q., Tao, D., et al., "Weak Predictability of Rupture Growth Evidenced by P Waves: Implications for Earthquake Early Warning," *Bulletin of the Seismological Society of America*, 112(5):2653-2667, 2022, doi:10.1785/0120210316.
6. Ji, C., Archuleta, R. J., Wang, Y., "Variability of Spectral Estimates of Stress Drop Reconciled by Radiated Energy," *Bulletin of the Seismological Society of America*, 112(4):1871-1885, 2022, doi:10.1785/0120210321.
7. Li, X., Li, N., Rong, M., et al., "Novel Evaluation Method for Site Effect on Earthquake Ground Motion Based on Modified Horizontal to Vertical Spectral Ratio," *Frontiers in Earth Science*, 10:938514, 2022, doi:10.3389/feart.2022.938514.
8. Ma, Q., Jin, X., Li, S. Y., et al., "Automatic P-Arrival Detection for Earthquake Early Warning," *Chinese Journal of Geophysics*, 56(7):2313-2321, 2013, doi:10.6038/cjg20130718.
9. Lior, I., Ziv, A., "Generic Source Parameter Determination and Ground-Motion Prediction for Earthquake Early Warning," *Bulletin of the Seismological Society of America*, 110(1):345-356, 2020, doi:10.1785/0120190140.
10. Wang, J., Ma, Q., Tao, D. W., et al., "Time-Domain Method of Source Parameters Considering Elliptic Model for $MW \geq 5.5$ Earthquakes," *Chinese Journal of Geophysics*, 67(3):1093-1107, 2024, doi:10.6038/cjg2023R0066.

11. Zhao, J. X., Hu, J., Jiang, F., et al., "Nonlinear Site Models Derived from 1D Analyses for Ground-Motion Prediction Equations Using Site Class as the Site Parameter," *Bulletin of the Seismological Society of America*, 105(4):2010-2022, 2015, doi:10.1785/0120150019.
12. Chandrakumar, C., Prasanna, R., Stephens, M., et al., "Earthquake Early Warning Systems Based on Low-Cost Ground Motion Sensors: A Systematic Literature Review," *Frontiers in Sensors*, 3:1020202, 2022, doi:10.3389/fsens.2022.1020202.
13. Peng, C., Ma, Q., Jiang, P., et al., "Performance of a Hybrid Demonstration Earthquake Early Warning System in the Sichuan–Yunnan Border Region," *Seismological Research Letters*, 91(2A):835-846, 2020, doi:10.1785/0220190101.
14. Asano, K., Iwata, T., "Source Rupture Processes of the Foreshock and Mainshock in the 2016 Kumamoto Earthquake Sequence Estimated from the Kinematic Waveform Inversion of Strong Motion Data," *Earth, Planets and Space*, 68:1-11, 2016, doi: 10.1186/s40623-016-0519-9.
15. Cremen, G., Galasso, C., Zuccolo, E., "Investigating the Potential Effectiveness of Earthquake Early Warning Across Europe," *Nature Communications*, 13(1):639, 2022, doi: 10.1038/s41467-021-27807-2.

Open Access This chapter is licensed under the terms of the Creative Commons Attribution-NonCommercial 4.0 International License (<http://creativecommons.org/licenses/by-nc/4.0/>), which permits any noncommercial use, sharing, adaptation, distribution and reproduction in any medium or format, as long as you give appropriate credit to the original author(s) and the source, provide a link to the Creative Commons license and indicate if changes were made.

The images or other third party material in this chapter are included in the chapter's Creative Commons license, unless indicated otherwise in a credit line to the material. If material is not included in the chapter's Creative Commons license and your intended use is not permitted by statutory regulation or exceeds the permitted use, you will need to obtain permission directly from the copyright holder.

